The Effect of Cell Size Distribution During the Cooling Stage of Cryopreservation without CPA

S. Fadda and A. Cincotti
Dipartimento di Ingegneria Chimica e Materiali, Università degli Studi di Cagliari, Piazza d'Armi, 09123 Cagliari, Italy

G. Cao
Dipartimento di Ingegneria Chimica e Materiali, Università degli Studi di Cagliari, Piazza d'Armi, 09123 Cagliari, Italy, and CRS4 (Center for Advanced Studies, Research and Development in Sardinia), Località Piscinamanna, Edificio 1, 09010 Pula, Cagliari, Italy

DOI 10.1002/aic.12137
Published online December 30, 2009 in Wiley InterScience (www.interscience.wiley.com).

A novel model capable of quantitatively describing and predicting intracellular ice formation (IIF) as a function of temperature in a cell population characterized by a size distribution is proposed. The model overcomes the classical approach which takes into account a population of identically sized cells. The size distribution dynamics of a cell population in response to water osmosis and IIF occurrence during the cooling stage of a standard cryopreservation protocol without using cryoprotective agent (CPA) is simulated by means of a suitable population balance approach. Specifically, the model couples the classical water transport equation developed by Mazur[1] to the quantitative description of nucleation and diffusion-limited growth of ice crystals in the framework of a 1-D population balance equation (PBE). It is found that IIF temperature depends on the cell size, i.e., it is higher for larger cells. Correspondingly, the probability of IIF (PIIF) results to be dependent on the initial size distribution of the cell population. Model's parameters related to the osmotic behavior of the cell population and to IIF kinetics are obtained by comparison between theoretical results and suitable experimental data of isolated rat hepatocytes available in the literature. Model reliability is successfully verified by predicting the experimental data of PIIF at different, constant cooling rates with better accuracy as compared to the theoretical approaches available in the literature. © 2009 American Institute of Chemical Engineers *AIChE J,* 56: 2173–2185, 2010

Keywords: cell number density distribution, population balance, intracellular ice formation, membrane permeability

Introduction

In the field of tissue engineering, cryopreservation of biological cells represents a current evolving technology where significant advances have been made to date, but several challenges remain.[2] Cryopreservation of cells involves cooling to subzero temperatures with or without CPAs, storage, thawing and return to physiological environment for specific usages. During freezing, ice initially forms in the extracellular medium surrounding the cells. As the extracellular ice grows, the extracellular solute concentration increases, thus, imposing a chemical potential difference between the cytoplasm and the unfrozen external solution which acts as driving force for water diffusion out of the cell through the

Correspondence concerning this article should be addressed to A. Cincotti at cincotti@dicm.unica.it and G. Cao at cao@visnu.dicm.unica.it.

plasma membrane, i.e., the osmotic transport. The rate of the osmotic water transport is limited by the permeability of the plasma membrane to water. Thus, the osmotic equilibrium can be maintained in a cooling process, only if the rate of cooling is sufficiently slow. On the other hand, if the time scales for the cooling process is short as compared to that one for membrane transport, low-temperatures are reached before significant dehydration takes place, and, thus, the cytoplasm becomes supercooled. In such a case, a driving force for IIF is established. Serious damage and injury, and even lethality occur during freezing due to IIF and ''solution effect'', i.e., membrane rupture, mechanical deformation, excessive cell dehydration, etc., taking place at high- and low-cooling rates, respectively.[3,4]

The development of cryopreservation protocols that guarantee cell survival is based[5] from one side on the use of CPAs, since the accidental discovery of glycerol,[6] which significantly prevent cell injury by reducing the intracellular concentration of water (i.e., the rate of formation of lethal ice), as well as the concentration of intracellular electrolytes which otherwise would increase due to water osmosis (i.e., protection against solution injury). From the other side, successful cryopreservation protocols can be developed by taking advantage of suitable mathematical models able to predict the behavior of cells during freezing, along the lines of the pioneering Mazur's work.[1]

Mechanistic models which simulate the behavior of a single cell during freezing-thawing processes have been proposed. In these models, osmosis was described on the basis of the bicompartmental transport Mazur's model,[1] while ice formation inside the cell was simulated according to the classical nucleation theory.[7] In particular, Karlsson et al.[8] developed a physicochemical theory of ice formation inside biological cells by coupling the water-transport model with the theory of ice nucleation and crystal growth. More recently, Gao and coworkers[9] proposed a modified version of Karlsson's model,[8] where the growing, time-dependent ice volume inside a cell during cooling is accounted for into Mazur's equation, thus, properly avoiding the underestimation of the intracellular salt concentration.

These models and other more sophisticated ones where nonideal, multicomponent liquid aqueous solutions are taken into account, are able to predict intracellular ice formation inside the cells as a function of cooling rate, seeding temperature, initial CPA concentration, and CPA type. However, in these modeling studies ice formation is either accounted for as taking place within a single representative (i.e., average) cell,[9] or the PIIF is related to the nucleation rate by assuming sporadic nucleation of identical cells.[10] On the other hand, it is difficult to accept on physical grounds that, a relatively high number of cells used during a standard cryopreservation protocols are identical, and that different temperatures of IIF for identical cells subjected to the same freezing cycle may be obtained due to a nucleation process stochastic in nature. Indeed, as already observed in the literature,[1] large cells are characterized by smaller surface-to-volume ratio than small ones, and, therefore, are expected to loose less water during the cooling stage. Consequently, at any given cooling rate, larger cells retain a higher percentage of internal water than small ones, so that supercooled conditions are reached earlier, i.e., at higher-temperatures.[1] According to this picture, a population of differently sized cells subjected to the same freezing protocol may exhibit different IIF temperatures. Specifically, one would expect that the IIF temperature of large cells is higher with respect to that one of small cells. In other words, PIIF should be related to the initial size distribution of a cell population.

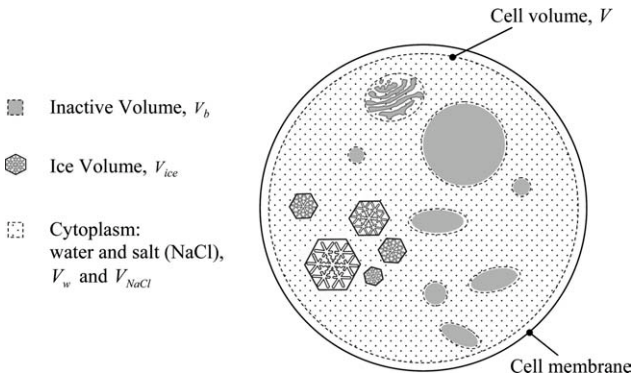

Figure 1. Schematic representation of the cell model.

Following these considerations, in this study, a novel model which simulates water osmosis and IIF occurrence during freezing of a cell population characterized by a size distribution is presented. Specifically, the model couples the classical water transport equation developed by Mazur[1] to the nucleation and diffusion-limited growth of ice crystals in the framework of a 1-D PBE which simulates the dynamics of a cell population volumic distribution during the cooling stage of a standard cryopreservation protocol without CPA. In addition, the model properly accounts for the liquid volume inside each cell when evaluating the ice nucleation rate.

Model equations

The proposed model is aimed to simulate the cooling stage of a population of spherical biological cells with a certain size distribution suspended in a water/sodium chloride solution. Each cell is modeled as surrounded by a semipermeable membrane, as depicted in Figure 1. Proteins, organelles and other macromolecules is representative of the cell volume V_b, which remains inactive to all physical processes considered in the proposed model. On the other hand, total cell volume V changes due to exosmosis of water occurring during freezing, as well as to intracellular ice crystal nucleation and growth. Water osmosis and IIF determine the corresponding variation of intracellular salt concentration, and, thus, of water and ice volumes, i.e., V_{water} and V_{ice}, respectively.

The model is based on the following assumptions:

- Cells are suspended in a solution whose initial conditions are isotonic;
- The extracellular solution is in thermodynamic equilibrium with extracellular ice seeded at a specific temperature T_{seed};
- Constant densities;
- Negligible difference between ice and liquid water densities;
- Constant osmotically inactive cell volume fraction v_b;
- Negligible impingement between intracellular ice crystals.

Model equations along with the corresponding initial and boundary conditions, are summarized in Table 1 for the sake of brevity. In particular, the system temperature is varied with time at a constant cooling rate, B starting from the initial value of 273.15 K (cf. Eq. 1). The dynamics of cell population volumic distribution during the cryopreservation protocol is quantitatively described by means of the 1-D PBE reported in Eq. 2 along with the corresponding initial and boundary conditions. Here, $n(V;t)$ represents the cell-number density distribution (i.e., $n(V;t)dV$ is the number of cells in the population that at time t possess a volume between V and $V+dV$), while $G_v(V)$ is the rate of cell volume variation (i.e., the so-called *growth rate*). Clearly, $n^0(V)$ refers to the initial (i.e., at isotonic condition) volume-size distribution of the cell population. N^0_{tot} is the initial total number of cells in the population. Basically, the integral boundary condition ensures that, during cooling, the total number of cells in the population does not change with time. On the other hand, a negative growth rate $G_v(V)$, due to water osmosis out of cell during cooling, shifts the cell-number density distribution $n(V;t)$ toward smaller volumes, thus, simulating cells shrinkage in a hypertonic environment. The rate of cell volume $G_v(V)$ variation may be evaluated by considering the classical Mazur's equation.[1] The latter one reported in Eq. 3 quantitatively describes the temporal variation of the total volume of every size class of the cell population driven by the osmotic gradient between intra- and extra-cellular solution concentrations expressed in terms of water mole fractions $x^{\text{int}}_{H_2O}$ and $x^{ext}_{H_2O}$, respectively. In particular, the logarithmic driving force appearing in Eq. 3 is valid if ideal, but not-dilute liquid solutions are assumed inside and outside the cells.[1,7] L_p represents the effective membrane permeability to water, which accounts for the effect of the two boundary layers in contact with the internal and external cell membrane surface, respectively.[11] In Eq. 3, $\Re$ and v_{H_2O} represent the universal gas constant and the molar volume of water, respectively, while A is the cellular membrane surface area.

It is apparent that, water osmosis rate, i.e., Eq. 3, simulates the temporal variation of any single-size class cell, by following its own temporal evolution from the initial volume to the final one. On the other hand, the continuous modeling framework represented by the PBE approach quantitatively describes the dynamics of the size distribution of the cell population by focusing on specific, fixed-class volumes which are reached, as time varies, by cells of different initial, isotonic volumes. Besides, a careful analysis of water osmosis rate equation reveals that volumic evolution of initial, differently sized cells never intersect, i.e., the relatively large and small cells of the initial population will always correspond to the relatively large and small cells of the current, shrinking-in-size population. Therefore, $G_v(V)$ in PBE and $\frac{dV}{dt}$ in Eq. 3 coincide, as indicated in the equations reported in Table 1, if referred to the same current, changing volume $V(t)$.[12]

The intracellular liquid molar fraction of water x^{int}_{H2O} appearing in Eq. 3 is determined by means of Eq. 4, where φ, assumed equal to 2, represents the dissociation constant of salt in water, while MW_{H_2O} and MW_{NaCl} are the molecular weight of water and salt, respectively. The intracellular salt wt % S^{int}_{NaCl} is calculated through Eq. 5, where ρ_{H_2O} is the pure water-mass density, c_0 is the isotonic concentration and V_0 the initial, isotonic cell volume.

The extracellular water molar fraction $x^{ext}_{H_2O}$ is evaluated through Eq. 6. Here $S_{eq}(t)$ representing the salt wt % at equilibrium in the extracellular solution, is obtained implicitly from the NaCl-H_2O liquidus line experimentally determined by Pegg[13,14] (cf. Eq. 7), at any system temperature smaller than T_{seed} down to the eutectic temperature T_e, (i.e., -21.2°C). Then, according to the binary phase-diagram of H_2O-NaCl, when the system temperature falls below T_e, in the extracellular medium assumed in thermodynamic equilibrium, the liquid phase is no longer present, and the cooling of pure ice and eutectic solid phase takes place. Correspondingly, the osmosis rate equation (cf. Eq. 3) vanishes at the eutectic temperature and below.

The classic Arrhenius-like temperature dependence[15] for the membrane permeability L_p is taken into account in Eq. 8, where E is the apparent activation energy for the permeation process and the pre-exponential factor $L_{p,ref}$ represents the value of permeability at a reference temperature chosen equal to 273.15 K.

A time invariant surface area A, equal to the area of the spherical cell under isotonic conditions, i.e., the area of a sphere with the initial volume V_0, is often considered in the literature. This corresponds to assume that, during water osmosis in a hypertonic environment, cell membrane does not shrink but folds itself, thus, preserving its ability to transfer water.[11] This simplifying assumption may be acceptable, even if not accurate, for several cell types. However, in this work, it seems more reasonable to assume that the effective surface area of a spherical cell of shrinking volume V, varies with time as stated by Eq. 9.

The intracellular liquid water volume V_{water} appearing in Eq. 5 may be evaluated through Eq. 10, where all the contributions to cell volume V, as depicted in Figure 1, are taken into account. It should be noted that, in order to fulfill the initial isotonic conditions, the salt volume is evaluated by accounting for the number of nonpermeant salt moles dissolved in the intracellular solution (cf. Eq. 12).

In order to determine the intracellular ice volume V_{ice} appearing in Eq. 10, the modeling of IIF for any size class cell of the considered population needs to be addressed. To this aim, it is worth noting that, when a freezing process is carried out without CPAs, like the one simulated in this work, internal ice nucleation takes place at relatively high-temperatures, i.e., when crystal growth is relatively fast. Therefore, the rapid ice-crystal growth in association with a small control volume (i.e., cell volume) generates only a very limited number of ice crystals inside any single cell of the population (typically no more than one, under several operative conditions considered in this work). This aspect clearly prevents the application of the PBE continuous modeling approach also for simulating ice nucleation and growth inside any size class of the cell population. Consequently, the evaluation of intracellular ice volume V_{ice} is performed through a discrete modeling approach by following the fate of any single ice nucleus that first forms, and then grows as time increases, inside any size class of the cell population. Specifically, in Eq. 13 shown in Table 1, V_{ice} is obtained by summing up the volumes of all the spherically growing ice crystals of radius $r_i(t)$ nucleated so far ($N_{\text{ice}}(t)$). The latter

Table 1. Model Equations

Cooling temperature dynamics

$$T(t) = 273.15 - B \cdot t \quad \text{or} \quad \begin{cases} T = 273.15 & t = 0 \\ T = T_{seed} & t > 0 \end{cases} \tag{1}$$

Cell population volumic distribution dynamics

$$\frac{\partial\, n(V;t)}{\partial t} + \frac{\partial[G_v(V) \cdot n(V;t)]}{\partial V} = 0 \quad \begin{cases} n(V;t) = n^0(V) & at \quad t = 0 \quad ; \quad \forall V \in [0, +\infty[\\ \int_0^{+\infty} n(V;t)\, dV = N^0_{tot} & \forall t \end{cases} \tag{2}$$

Osmotic water transport dynamics

$$T_e \le T \le T_{seed}$$

$$\frac{dV}{dt} = G_v(V) = -\frac{L_p(t) \cdot A(t) \cdot \Re \cdot T(t)}{v_{H_2O}} \quad \ln\left(\frac{x^{\text{int}}_{H_2O}(t)}{x^{ext}_{H_2O}(t)}\right) ; \quad V = V_0 \quad at \quad t = 0 \tag{3}$$

$$x^{\text{int}}_{H_2O}(t) = \left[\varphi \frac{MW_{H_2O}}{MW_{NaCl}} \left(\frac{S^{\text{int}}_{NaCl}(t)}{100 - S^{\text{int}}_{NaCl}(t)}\right) + 1\right]^{-1} \tag{4}$$

$$S^{\text{int}}_{NaCl}(t) = \frac{c_0 \cdot V_0 \cdot (1 - v_b) \cdot MW_{NaCl}}{c_0 \cdot V_0 \cdot (1 - v_b) \cdot MW_{NaCl} + \rho_{H_2O} \cdot V_{water}(t)} \times 100 \tag{5}$$

$$x^{ext}_{H_2O}(t) = x^{eq}_{H_2O}(t) = \left[\varphi \frac{MW_{H_2O}}{MW_{NaCl}} \left(\frac{S_{eq}(t)}{100 - S_{eq}(t)}\right) + 1\right]^{-1} \tag{6}$$

$$T(t) = 273.15 - (0.6) \cdot S_{eq}(t) - \left(1 \times 10^{-3}\right) \cdot S^2_{eq}(t) - \left(4.5 \times 10^{-4}\right) \cdot S^3_{eq}(t) \tag{7}$$

$$L_p(t) = L_{p,ref} \cdot \exp\left(-\frac{E}{\Re}\left(\frac{1}{T(t)} - \frac{1}{273.15}\right)\right) \tag{8}$$

$$A(t) = 4\pi \cdot \left(\frac{3}{4\pi}\right)^{2/3} \cdot V(t)^{2/3} \tag{9}$$

Intracellular liquid water volume

$$V_{water}(t) = V(t) - V_b - V_{ice}(t) - V_{NaCl} \tag{10}$$

$$V_b = v_b \cdot V_0 \tag{11}$$

$$V_{NaCl} = v_{NaCl} \cdot n_{NaCl} = v_{NaCl} \cdot c_0 \cdot (1 - v_b) \cdot V_0 \tag{12}$$

Intracellular ice mass balance

$$V_{ice}(t) = \begin{cases} 0 & if \quad N_{ice}(t) = 0 \\ \sum_{i=1}^{N_{ice}(t)} \frac{4\pi}{3} [r_i(t)]^3 & if \quad N_{ice}(t) \ge 1 \end{cases} ; \qquad N_{ice}(t) = \text{int}\left(\overline{N}_{ice}(t)\right) \tag{13}$$

Nucleation and growth of intracellular ice crystals

$$\frac{d\bar{N}_{ice}}{dt} = B_0(t) \quad ; \quad \bar{N}_{ice} = 0 \qquad at \qquad t = 0 \tag{14}$$

$$B_0(t) = J(t) \cdot (V(t) - V_b - V_{ice}(t)) \tag{15}$$

$$J(t) = J_0 \cdot D(t) \cdot \exp\left(-\frac{E_N(t)}{k_B \cdot T(t)}\right) \tag{16}$$

$$E_N = \frac{4}{3}\pi \cdot \gamma \cdot r^{*^2} \tag{17}$$

$$r^*(t) = \frac{2 \cdot \gamma \cdot v_{ice}}{\Re \cdot T(t) \cdot \ln\left(\frac{x^{\text{int}}_{H_2O}(t)}{x^{eq}_{H_2O}(t)}\right)} \tag{18}$$

$$D(t) = \frac{k_B \cdot T(t)}{6\pi \cdot a_0 \cdot \eta(t)} \tag{19}$$

$$\eta(t) = \eta_w(t) \cdot \exp\left(\frac{k_e \cdot \phi_s\left(S^{\text{int}}_{NaCl}\right)}{1 - Q \cdot \phi_s\left(S^{\text{int}}_{NaCl}\right)}\right) \tag{20}$$

$$\phi_s\left(S^{\text{int}}_{NaCl}\right) = \frac{v_{NaCl} + h \cdot v_{H_2O}}{\frac{MW_{NaCl}}{\rho_{H_2O}}\left(\frac{100}{S^{\text{int}}_{NaCl}(t)} - 1\right) + v_{NaCl}} \tag{21}$$

Table 1. (*Continued*)

$$\eta_w(T) = A_w \cdot \left(\frac{T(t)}{225} - 1\right)^{\mu} \quad ; \quad T > 225\ K \tag{22}$$

$$\begin{cases} r_i(t) = 0 \quad at \quad t < t_i \quad when \quad N_{ice}(t) = 0 \\ \frac{dr_i}{dt} = \bar{D}(t) \cdot \frac{\Omega_g(t)}{r_i} \quad ; \quad r_i(t) = r^*(t) \quad at \quad t = t_i \quad \forall i \in [1; N_{ice}(t)] \end{cases} \tag{23}$$

$$\Omega_g(t) = \frac{x^{\text{int}}_{H_2O}(t) - x^{eq}_{H_2O}(t)}{1 - x^{eq}_{H_2O}(t)} \tag{24}$$

$$\bar{D}(t) = \sqrt{D(t) \cdot D_{eq}(t)} \tag{25}$$

$$\eta_{ice}(t) = \frac{V_{ice}(t)}{V(t) - V_b} \tag{26}$$

$$PIIF(t) = \frac{\int_0^{+\infty} n(V;t)|_{\eta_{ice} \geq 50\%}\, dV}{N^0_{tot}} \tag{27}$$

one may be evaluated from the knowledge of the ice nucleation rate in a cell (B_0) as shown in Eq. 14, where the absence of ice crystals inside any size class of the cell population is guaranteed by the initial condition. In addition, since Eq. 13 is based on a discrete modeling approach $N_{\text{ice}}(t)$, has to be a natural number. Consequently, it is evaluated by truncating (to the smallest near integer) the real number $\overline{N}_{\text{ice}}(t)$ obtained upon integration of Eq. 14.

Following the classical nucleation theory[16] which defines a specific nucleation rate J (i.e., number of nuclei formed in a unit time per unit of liquid volume), the ice nucleation rate B_0 can be expressed as proportional to the liquid volume inside a cell, as shown in Eq. 15 of Table 1. It is worth noting that, even if Zhao et al.[9] properly improved the determination of osmotic driving force in Mazur's equation by taking into account V_{ice} when evaluating the nucleation rate, the sum of intracellular liquid volume and ice volume inside the cells was considered as control volume.

The specific nucleation rate J is given by Eq. 16, while the corresponding activation energy of nucleation E_N may be obtained from Eq. 17, being the critical radius r^* given by Eq. 18. According to Dirksen and Ring,[16] the rate of heterogeneous nucleation has the same form as the homogeneous one (i.e., on a per volume basis), being the difference only related to the specific value of the surface energy.

It is worth noting at this point that, while water osmosis stops when the system temperature reaches the eutectic value, IIF still takes place. Indeed, while extracellular medium is assumed under thermodynamic equilibrium conditions, this is not true for intracellular liquid and solid phases. Consequently, nucleation and ice-crystal growth driving forces need to be determined even at temperatures below the eutectic point. Under these conditions, following Zhang and Stangle[17] and Locci et al.,[18] $x^{eq}_{H_2O}(t)$ is determined by extending the liquidus line of the NaCl-H_2O binary phase diagram (cf. Eq. 7) down to -40°C, thus considering a metastable liquidus line.

The diffusivity of water appearing in Eq.16 is determined through the Stokes-Einstein equation reported in Eq. 19 shown in Table 1. Solution viscosity is evaluated as shown in Eq. 20 of Table 1, according to the model developed by Vand[19–21] for water-NaCl solutions. The volume fraction of hydrated salt ions suspended in the continuous water medium ϕ_s is determined as reported in Eq. 21 of Table 1. The effective number of water molecules in the hydration shell of salt molecule, h is a very important parameter, as it influences cytoplasm solution viscosity, and, indirectly, IIF. Unfortunately, since no equations are available in the literature to express the dependence of h as a function of temperature and intracellular salt concentration,[9] in this work, it is assumed constant and equal to 1.

For the temperature-dependence of pure water viscosity $\eta_w(T)$ appearing in Eq. 20, the phenomenological (power-law) viscosity model developed by Taborek et al.[22] is used (cf. Eq. 22 in Table 1).

Finally, in order to determine the intracellular ice volume V_{ice} using Eq. 13, the temporal evolution of the radius of the i-th ice crystal ($r_i(t)$) needs to be evaluated. To this aim, the classical *diffusion-controlled growth* law[16] is taken into account, as reported in Eq. 23 shown in Table 1, where t_i is the birth instant of the i-th ice nucleus, which starts growing from the actual initial critical radius $r^*(t_i)$. Basically, for any size class of the cell population, t_i corresponds to the time instant when the natural number $N_{\text{ice}}(t_i)$ increases. It is worth noting that, at any given size class of the cell population, internal ice nuclei are formed at different times (t_i), starting from different critical size $r^*(t_i)$, and with different initial growth rates ($\left(\frac{dr_i}{dt}\right|_{t_i} = \bar{D}(t_i) \cdot \frac{\Omega_g(t_i)}{r^*(t_i)}$). According to Zhang and Stangle[17], the driving force of ice crystal growth is evaluated as reported in Eq. 24, while the effective diffusivity of water $\overline{D}$ is calculated for the sake of simplicity on the basis of Eq. 25. Here, $D_{eq}(t)$ corresponds to the water diffusivity given by Eq. 19 when the intracellular solution viscosity η is evaluated at a salt wt % content equal to $S_{eq}(t)$. Indeed, due to the concentration gradient that drives the *diffusion-controlled growth*, an average value of water diffusivity along the diffusion path needs to be evaluated.

In the next section, model results will be discussed and analyzed also by considering suitable experimental data

available in the literature.[10] Specifically, the temperature at which IIF occurred experimentally under given freezing conditions was determined from the darkening of the cell due to the light scattering from small ice crystals forming inside the cells. The number of iced-up cells is then evaluated using a cryomicroscopic system. The corresponding PIIF is computed at each temperature level as the fraction of cells with respect to the total initial ones cumulatively frozen at that temperature. The value of PIIF at the temperature of $-40°C$ is then reported as a function of different cooling rates.[10] In order to make an appropriate comparison with these experimental data, in this work it is assumed that cells are iced-up when the ice volume percentage defined through Eq. 26, as reported in Table 1, reaches the value of 0.5. In the following section, the reliability of such a choice will be analyzed. Correspondingly, in this work the PIIF is defined as shown in Eq. 27 of Table 1. It is apparent that the PIIF definition introduced in this work is related to the corresponding experimental quantity. In fact, while the denominator represents the total number of cells, the numerator apparently displays a cumulative character, thus, providing the cells cumulatively "frozen" at the given temperature. It is worth noting that, while in previous models based on sporadic nucleation, the PIIF may be defined for a system composed of identical biological cells only when crystallization (i.e., crystal growth) time is negligible with respect to the nucleation time[7] (i.e., a single ice nucleus per cell is formed), the deterministic approach adopted in our work permits to provide a more general definition of PIIF, i.e., independently from the number of nuclei inside cells. This way, a comparison with experimental data in terms of PIIF can be made even if more than one ice nucleus is formed inside a single cell. Thus, the structure of our model falls well within the lines very recently drawn on this aspect by Karlsson.[23]

Numerical solution

The equations of the proposed model are solved numerically as a time-dependent problem. The system of equations consists of complexly coupled algebraic and differential equations. In particular, Eqs. 1, 10 and 13 are explicit algebraic equations used to evaluate the system temperature, water, and ice volume in any size class of the cell population, respectively. Equation 7 is an implicit algebraic equation (solved by Newton's method) that provides the wt % content of salt in the extracellular liquid solution. Eqs. 3, 14 and 23 are ordinary differential equations (integrated as an initial value problem by means of standard numerical libraries, DIVPAG, IMSL), which provide total cell volume, number of ice crystals, and the size of every ice crystals in any size class of the cell population, respectively. Finally, Eq. 2 is a partial differential equation (in the variables t and V) used to calculate the size distribution of the cell population. It is solved through the method of lines[24] by discretizing only the partial derivative with respect to V using a constant step-size mesh. Typically, 1000 fixed-grid points are used, since finer grids do not provide significant improvements in accuracy. Thus, the partial differential equation (Eq. 2) is reduced to a system of ordinary differential equations in time, which is integrated as an initial value problem by means of standard numerical libraries (DIVPAG, IMSL), along with the remaining ordinary differential equations of the proposed model. All integrals along the V domain appearing in model equations are numerically evaluated by means of trapezoid rule.

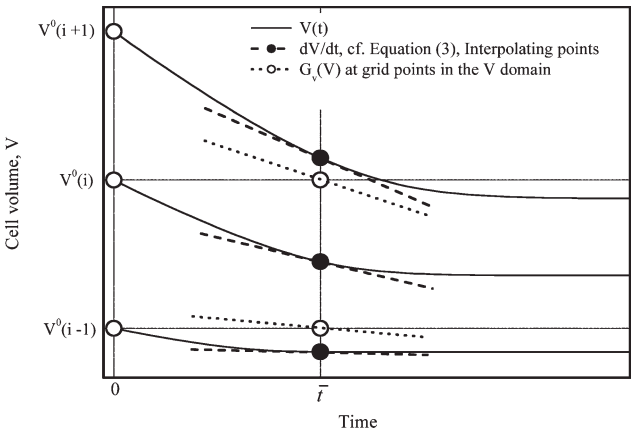

Figure 2. Discretization grid in the cell volume domain for integrating PB in Eq. 2.

In the framework of the method of lines, the determination of $G_v(V)$ in Eq. 2 from $\frac{dV}{dt}$ in Eq. 3 deserves a comment. Indeed, according to the discretization of the partial derivative along the V domain of the PBE, at any time $\bar{t}$ of temporal integration, $G_v(V)$ needs to be evaluated at the nodal, fixed discretization points, as schematically depicted in Figure 2. However, the volume trajectories of any size class of the cell population obtained by integrating Eq. 3 may not coincide with the chosen nodal, fixed discretization points at any time during the temporal integration. For this reason $G_v(V)$ in the nodal, fixed discretization points is determined by a simple linear interpolation between the nearest volume trajectories, as shown in Figure 2.

Results and Discussion

The mathematical model proposed in this work is applied to quantitatively describe and predict IIF taking place in a cell population characterized by a size distribution during the cooling stage of a standard cryopreservation protocol where no CPA is used. Model reliability is verified by comparing theoretical results and the experimental data related to isolated rat hepatocytes reported by Toner et al.[10] In particular, the experimental data considered in this work to determine the values of the adjustable parameters of the proposed model are related to a population constituted by a sufficiently high number of cells for which the application of a PBE approach seems reasonable. However, cryomicroscopic experimental data in terms of PIIF during cooling are typically obtained by observing the behavior of a restricted number of cells, and without providing the initial, isotonic cell-diameter distribution. On the other hand, the latter information is reported by Toner et al.[10] and is shown in Figure 3. It represents a histogram (frequency) distribution $N^0(L)$ along cell diameter L related to 91 cells at ambient temperature under isotonic conditions. The corresponding cell-number density distribution as a function of cell volume, which represents the initial condition $n^0(V)$ of Eq. 2 reported in

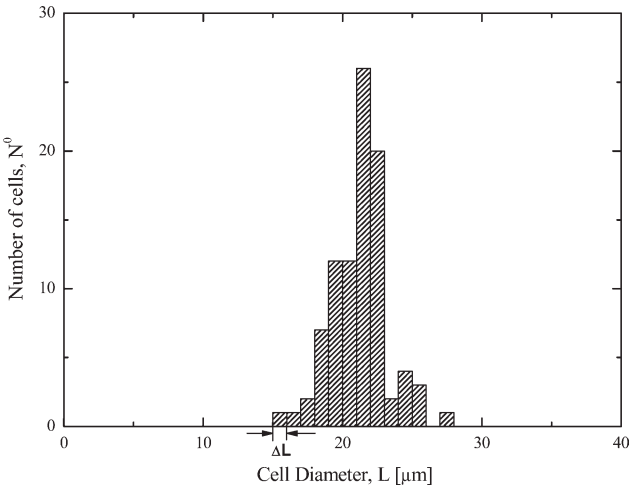

Figure 3. Diameter distribution of isolated rat hepatocytes in DMEM at 22°C (adapted from Toner et al.[10]).

Table 1, may be readily calculated from the experimental histogram reported in Figure 3, as $n^0(V) = \frac{N^0(L)}{\Delta L} \cdot \frac{2}{\pi} \cdot \frac{1}{L^2}$, where L is the average diameter in the corresponding histogram interval ΔL. The obtained results are then suitably interpolated as reported in Figure 4a, through standard cubic spline functions.

Since one of the primary aims of this work is to demonstrate that IIF taking place during a standard cryopreservation protocol results to be dependent on the initial size distribution of a cell population, two additional fictitious, narrow, initial cell-number density-distributions $n_1^0(V)$ and $n_2^0(V)$, will be also considered, as reported in Figure 4b. It is apparent from Figure 4 that the two fictitious distributions are characterized by mean values which correspond to the smallest and the largest size class cells of the experimental distribution, respectively. These narrow distributions, indeed, have been adopted as initial conditions of the proposed model in order to highlight the different behavior of large and small cells with respect to the experimental distribution shown in Figure 4a.

As reported in Table 2, the proposed model contains a large number of parameters. In particular, five of them (i.e., $L_{p,ref}$, E, v_b, J_0 and γ) are obtained by direct comparison with experimental data, following the procedure described next, while the remaining ones are taken from the literature. Ideally, the reliable evaluation of the five adjustable parameters mentioned previously, three of which (i.e., $L_{p,ref}$, E, and v_b) are characteristic of water osmosis of the specific cell lineage at hand, while J_0 and γ are related to IIF kinetics, should be obtained independently using specifically designed experimental runs. In particular, the temporal evolution of the size distribution of the adopted cell lineage population should be first measured by an electronic particle-size counter[27,28] at relatively high-temperatures in order to prevent ice formation. Thus, the characteristic parameters related to the water osmosis, could be determined by direct comparison between these experimental data and a simplified version of the proposed model where IIF is neglected.[28] Next, the remaining parameters related to the ice nucleation could be evaluated through a standard fitting procedure of suitable cryomicroscopic experimental data in terms of PIIF during cooling of a relatively abundant population of cells against the complete version of the proposed model, where the osmotic parameters are maintained fixed as previously obtained.

Unfortunately, since, to the best of our knowledge, an entire set of experimental data of the type described previously is not available in the literature, in this work all the five adjustable parameters are evaluated simultaneously by direct comparison between the complete version of the proposed model and the PIIF experimental data of 60 isolated rat hepatocytes when a cooling rate of −400°C/min is used.[10] The value of the parameters obtained by means of a standard fitting procedure based on least-squares minimization is reported in Table 2, while the comparison between model results and experimental data is shown in Figure 5. As it can be seen, a good agreement is achieved; being the average percentage error obtained during the fitting procedure equal to about 10%. In particular, the proposed model is able to simulate the completion of IIF at −400°C/min in the temperature range (−5°C ÷ −15°C), when the initial cell-size distribution reported in Figure 4a is considered. On

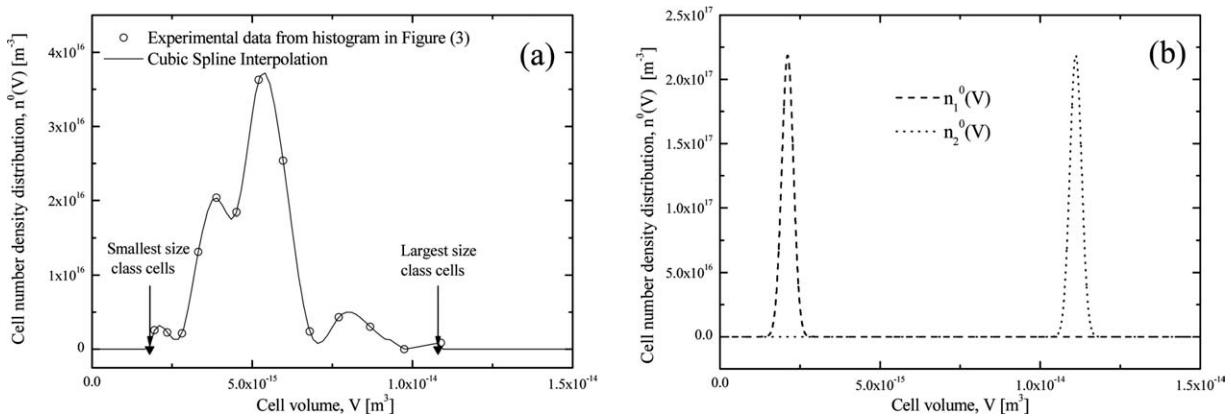

Figure 4. Initial conditions for Eq. 2: experimental and interpolated cell-number density distribution as a function of cell volume obtained from Figure 3 (a), and narrow-number density distributions of fictitious populations of small and large cells (b).

Table 2. Model Parameters

Parameter	value	unit	reference
a_0	1.4×10^{-10}	$[m]$	[25]
A_w	0.139×10^{-3}	$[kg\ m^{-1}\ s^{-1}]$	[7]
c_0	142.5	$[mol\ m^{-3}]$	[10]
E	2.15×10^{5}	$[J\ mol^{-1}]$	This work (tuned parameter)
h	1	[—]	This work
J_0	1.75×10^{24}	$[\#\ m^{-5}]$	This work (tuned parameter)
k_e	2.5	[—]	[7]
$L_{p,ref}$	7.82×10^{-13}	$[m^3\ N^{-1}\ s^{-1}]$	This work (tuned parameter)
N_{tot}^0	91	[—]	[10]
Q	0.61	[—]	[7]
T_e	251.95	$[K]$	[13,14]
T_{seed}	272.15	$[K]$	[10]
v_b	0.465	[—]	This work (tuned parameter)
v_{H_2O}	1.8×10^{-5}	$[m^3 \cdot mol^{-1}]$	[26]
v_{ice}	19.65×10^{-6}	$[m^3 \cdot mol^{-1}]$	[26]
v_{NaCl}	2.69×10^{-5}	$[m^3 \cdot mol^{-1}]$	[26]
γ	1.043×10^{-3}	$[J\ m^{-2}]$	This work (tuned parameter)
μ	−1.64	[—]	[7]
ρ_{H_2O}	10^6	$[g \cdot m^{-3}]$	[26]

the contrary, by adopting the two fictitious initial distributions reported in Figure 4b, while keeping constant all the other parameters and operative conditions of the experimental run, the PIIF vs. system temperature simulated by the proposed model is completely different. Indeed, the model predicts no IIF down to −16°C for the case of the narrow, small-size distribution of the cell population, while an abrupt increase of PIIF takes place around −5.5°C, for the case of the narrow, large-sized cell population. Thus, differently sized cells in a population exhibit a different IIF temperature under the same operative conditions. Specifically, the temperature of IIF is higher for the larger cells and, correspondingly, smaller cells are less prone to IIF. Moreover, the obtained values of the osmotic parameters (i.e., $L_{p,ref}$, E, and v_b) reported in Table 2 are similar to those reported in the literature.[10] On the other hand, the obtained values of parameters J_0 and γ related to IIF kinetics cannot be directly compared to the two ones typically determined in the literature, since a different modeling approach with diverse mathematical relationships has been adopted for the nucleation rate. On the other hand it is worth noting that, when comparing our approach to previous ones, the tuned parameters of the proposed model are determined as invariant with the imposed cooling rate. In fact, it is difficult to accept on physicochemical grounds that the parameters of previous models may be determined as dependent on cooling rate, even if average values are then used during simulations.[10]

On the basis of the results shown above, the reliability of the proposed model is then tested by predicting the experimental run reported in Figure 6. Here, the fractional cell volume at a constant holding temperature of −1.1°C (= T_{seed})

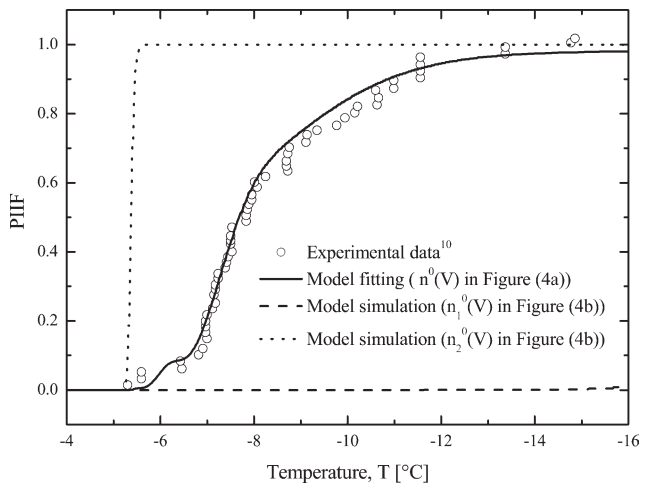

Figure 5. Comparison between experimental PIIF for a population of rat hepatocytes cooled at −400°C/min, and model result (solid line), along with model simulations performed using the fictitious initial narrow distributions of small (dashed line), and large cells (dotted line).

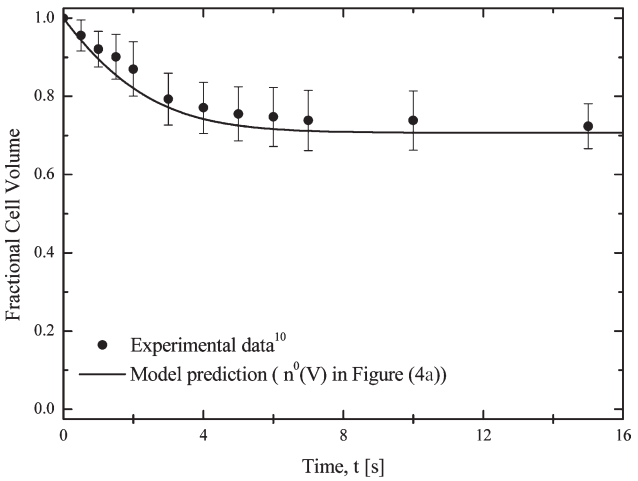

Figure 6. Comparison between experimental data and model predictions in terms of temporal behavior of the average fractional volume of isolated rat hepatocytes cooled at a constant temperature of −1.1°C in the presence of extracellular ice.

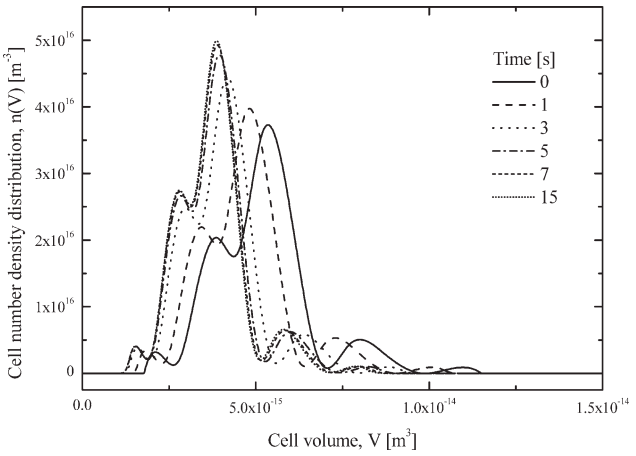

Figure 7. Model results in terms of temporal evolution of the number density distribution of a rat hepatocytes population cooled at a constant temperature of −1.1°C in the presence of extracellular ice.

is reported as experimentally measured by microscopically observing the behavior of seven cells. Clearly, in the proposed model applied to simulate these experimental data, the temperature initially at ambient value, is changed at $t > 0$, and kept constant at −1.1°C as reported in Eq. 1 of Table 1. Specifically, the average fractional volume of the cell population characterized by a size distribution and calculated by the proposed model as $\frac{\int_0^{+\infty} V \cdot n(V;t)dV}{\int_0^{+\infty} V \cdot n^0(V)dV}$, is compared in Figure 6 with the experimental data taken from literature. It may be seen that a good matching is obtained, thus, showing the prediction capability of the proposed model. Additionally, due to the relatively high-system temperature, IIF does not really take place during this experimental run, and, accordingly, the proposed model predicts no ice nucleation and growth inside any size class of the cell population. The corresponding temporal evolution of the cell-number density distribution predicted by the proposed model is shown in Figure 7. Clearly, cells move to the left side of the volume distribution (i.e., toward smaller volumes), since, due to ice seeding, the extracellular solution becomes hypertonic with respect to the intracellular one, thus, inducing cell shrinkage via water osmosis.

The predictive model capability has been further tested by comparing experimental data with model results in terms of PIIF at −40°C as a function of the cooling rate. The cumulative fractional number of cells that underwent IIF at −40°C reported in Figure 8 is predicted with a reasonable accuracy when the cell-size distribution reported in Figure 4a is adopted. The matching is definitely better than the one obtained by the model proposed by Toner et al.[10] where a sporadic nucleation in a population of identically sized cells is assumed. In particular, an abrupt increment of $PIIF|_{-40°C}$ at about −100°C/min is predicted by Toner et al.[10] Interestingly, this behavior could be obtained by the model here proposed if a population of identically sized cells was taken into account. For this reason, the predictions of the proposed model, when adopting the distributions $n_1^0(V)$ and $n_2^0(V)$ shown in Figure 4b, are also plotted. In particular, at −40°C the population of large cells is completely iced-up in a narrow range of applied cooling rates, i.e., (−30°C/min ÷ −60°C/min), while a faster temperature gradient (i.e., −200°C/min) is necessary to induce IIF in the small cells distribution, even if only 7% of total cell number is frozen.

Finally, the predictive capability of the proposed model is verified by comparison with the temporal profiles of the fractional cell volume measured at different cooling rates,[10] as reported in Figure 9. In particular, at −6°C/min (cf. Figure 9a) the modeled temporal profiles of the average fractional cell volume obtained when adopting as $n^0(V)$ in Eq. 2, the experimentally determined initial cell-size distribution (cf. Figure 4a), as well as the narrow small and large-size cell distributions (cf. Figures 4b, $n_1^0(V)$ and $n_2^0(V)$, respectively) are coincidental, and a good matching with experimental data is obtained. However, at higher-cooling rates (cf. Figure 9b–f)), the fractional cell volume corresponding to the three initial distributions mentioned previously display a different behavior. Specifically, at cooling rates between −50°C/min and −400°C/min, the temporal profile of the fractional cell volume obtained with the large-size cell distribution $n_2^0(V)$, as the initial one greatly overestimates the experimental data. On the other hand, by adopting the experimentally determined initial cell-size distribution reported in Figure 4a, at −50°C/min (cf. Figure 9b), the model prediction still reasonably agrees with the experimental data, while, at higher cooling rates, it overestimates them (cf. Figure 9c–f)). However, if the small-size cell distribution $n_1^0(V)$, depicted in Figure (4b), is taken into account, at any cooling rate the proposed model shows a good prediction capability of the experimental data. It is worth noting that, at −400°C/min, model results obtained from the different initial cell-size

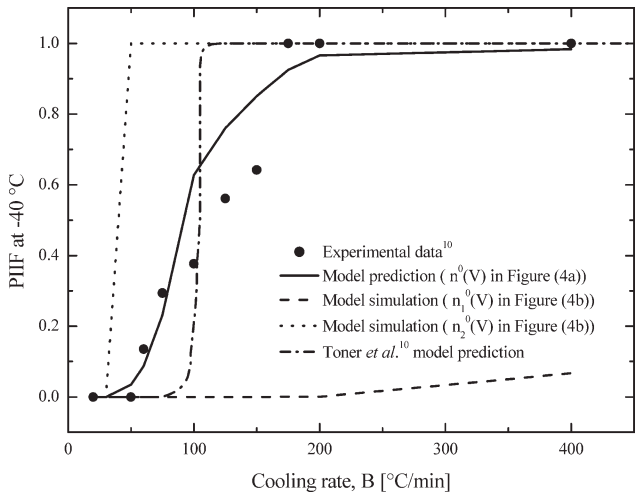

Figure 8. Comparison between experimental data and model predictions (solid line) in terms of PIIF at −40°C for a population of rat hepatocytes as a function of cooling rate, along with model simulations performed using the fictitious initial narrow distributions of small (dashed line) and large cells (dotted line), as well as the related results obtained in the literature.

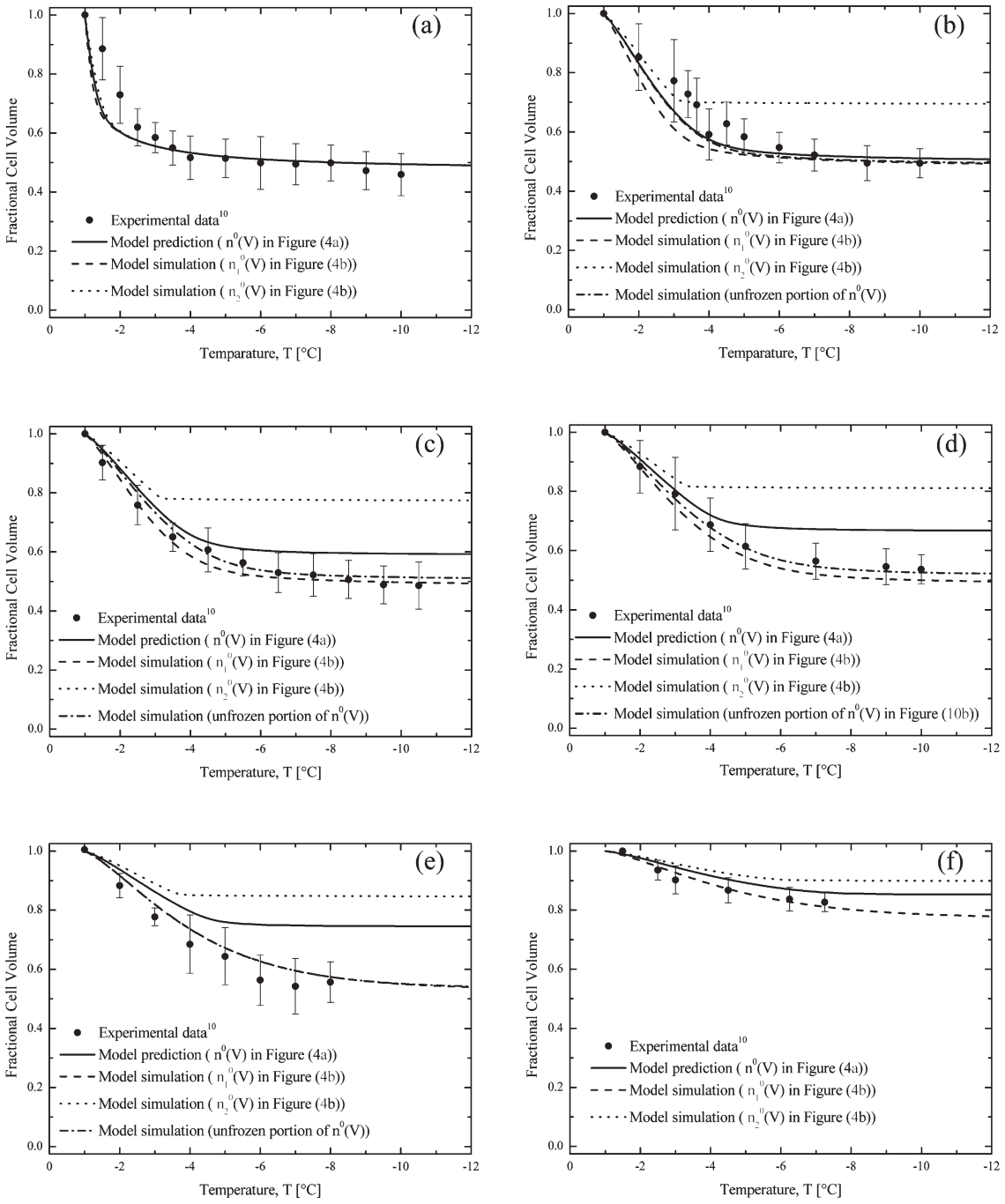

Figure 9. Comparison between experimental data and model predictions, obtained using different initial cell-size distributions, in terms of temporal behavior of the average fractional volume of isolated rat hepatocytes cooled in the presence of extracellular ice at −6°C/min (a), −50°C/min (b), −75°C/min (c), −100°C/min (d), −150°C/min (e), and −400°C/min (f), respectively.

distributions (cf. Figure 4) are similar if compared to those ones obtained at relatively lower cooling rates, while, apparently, a better matching with experimental data results.

The reason why our model shows a reasonable predictive capabilities in a wide range of operative conditions except for those ones reported in Figure 9c–f, when using the initial cell-size density distribution $n^0(V)$ shown in Figure 4a may be explained. To this aim, the interplay between water osmosis and IIF kinetics, and the effect of the size distribution on these coupled phenomena as a function of the cooling rate need to be more deeply analyzed. First of all, it is well known in the literature[1] that more significant water osmosis takes place when a lower cooling rate is applied. In particular, in the system considered in this work, cell shrinkage occurs until a temperature of −10°C (i.e., far from the eutectic point of −21.2°C) is reached, for the various cooling

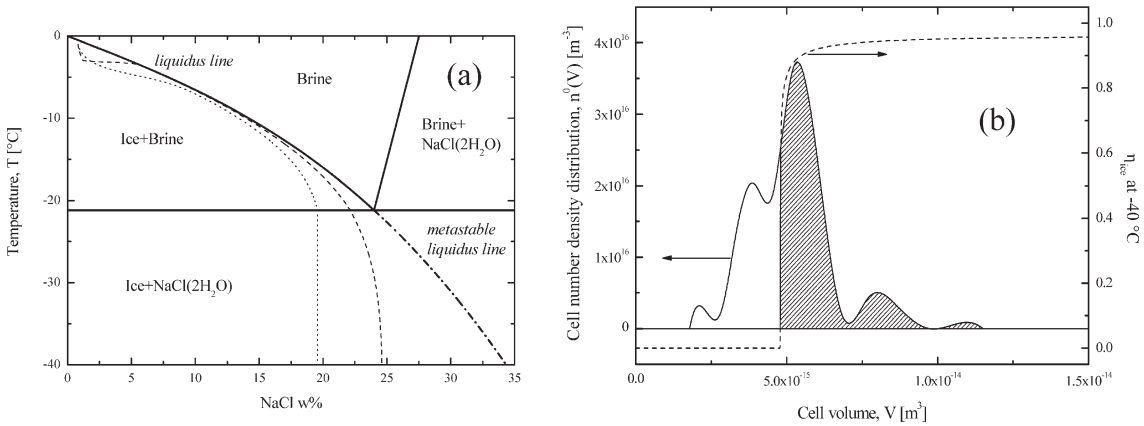

Figure 10. Binary water-NaCl phase diagram where the computed sodium chloride weight percentage S^{int}_{NaCl} corresponding to the smallest (dotted line), and the largest class size cells (dashed line) depicted in Figure 4a is reported for the case of cooling rate of −100°C/min (a), and corresponding cell-size distribution, and internal ice volume percentage distribution $\eta_{ice}|_{-40°C}$ as a function of initial cell volume, where frozen and unfrozen cells are indicated by the shadowed and the white areas, respectively (b).

rates considered in Figure 9. This is clearly due to the Arrhenius-like temperature dependence of membrane permeability (cf. Eq. 8 in Table 1). As cooling rate increases, the rapid variation of temperature quickly reduces the membrane permeability, so that a significant dehydration cannot take place. As a result, the cytoplasm tends to reach a supercooled state, and IIF occurs inside an increasing number of cells, starting from the larger ones and, subsequently, involving smaller cells (cf. Figure 8). IIF occurrence reduces exchangeable water, and further limits the osmosis phenomenon by lowering the corresponding driving force. Accordingly, the fractional cell-volume variation reported in Figure 9f is less pronounced than the corresponding one reported in Figure 9a, where IIF does not take place. On the other hand, the average fractional cell volume obtained at −400°C/min still varies of about 15% down to −7°C. Thus, the choice to determine both the osmotic, as well as the IIF related adjustable parameters of the proposed model by comparison with the experimental data given in Figure 5 seems appropriate, since system behavior is simultaneously affected by both phenomena.

To better describe the effect of the cell-size distribution on the interplay between water osmosis and IIF kinetics, we consider the smallest and the largest size class cells of the initial population shown in Figure 4a. The corresponding intracellular sodium chloride weight percentage S^{int}_{NaCl} obtainable through our model are reported on the relevant phase diagram as a function of temperature in Figure 10a for the case of cooling rate equal to −100°C/min, which is taken as representative, for the sake of brevity, of the different cooling rates investigated. It may be seen that, largest and smallest size class cells show a different path in terms of S^{int}_{NaCl}. Specifically, for the case of largest size class cells, the occurrence of IIF may be recognized from the relatively abrupt slope change of the corresponding path (dashed line), taking place at about −3°C, toward higher salt concentration values. Since ice is formed inside largest size class cells, the intracellular salt concentration rapidly increases, thus, reaching a final intracellular salt concentration higher than that one of the smallest size class cells, as it may be seen from Figure 10a. As a consequence of the simultaneous occurrence of IIF and osmosis, the computed sodium chloride weight percentage profile of the largest size class cells significantly overlaps with the liquidus line. A similar behavior is obtained when varying the cooling rate, except for the case of −6°C/min, where ice is not formed at all. On the other hand, for the case of the smallest size class cells only osmotic phenomenon takes place. The latter one is then responsible, as temperature decreases, for the increase of the computed sodium chloride weight percentage, which eventually stops at the eutectic temperature and below, as assumed by our model. When cooling rate is decreased or increased from the value of −100°C/min (cf. Figure 10a), if IIF does not occurs, the final salt concentration inside smallest size class cells increases or decreases, respectively, since water osmosis is correspondingly augmented or slowed down.[1]

The selective character of IIF depending on the size distribution of a cell population is further addressed in Figure 10b, where, for the cooling rate of −100°C/min, the initial cell-size distribution $n^0(V)$ (cf. Figure 4a) is shown along with the corresponding internal ice volume percentage distribution $\eta_{ice}|_{-40°C}$ (cf. Eq. 26 in Table 1), reported as a function of initial cell volume. According to the proposed model, cells are considered iced-up when the corresponding η_{ice} is $\geq$ 50%. On the basis of this assumption, the shadowed portion of the initial cell-size distribution which corresponds to the iced-up cells at −40°C may be identified in Figure 10b. It is apparent that, if the choice of $\eta_{ice} \geq 50\%$ to establish ice formation would have been different, the shadowed portion would not change significantly due to the characteristic η_{ice} sharp step profile. Along these lines, the unfrozen portion at −40°C of the experimental, initial cell-size distribution may be identified by its nonshadowed portion. Clearly, as the cooling rate is decreased or increased from the value of −100°C/min (cf. Figure 10b), the frozen portion of the cell-size distribution decreases or increases, respectively. In particular, for the cases of −6 °C/min or −400°C/min the unfrozen portion coincides with the entire cell-size

distribution or, cannot be identified, respectively, since at $-40^{\circ}C$ the initial cell-size distribution results to be completely unfrozen or frozen, correspondingly.

When the corresponding unfrozen portion of initial cell-size distribution is taken as $n^0(V)$ in Eq. 2, in order to solve the proposed model, the corresponding predictions in terms of average fractional cell volume reported in Figure 9 (dash-dotted lines) are obtained. It may clearly be seen that the proposed model is now able to quantitatively interpret the experimental data with better accuracy, as compared to the case when the entire initial cell-size distribution (cf. Figure 4a) is taken into account. Thus, according to the proposed model, the experimental data considered in Figure 9 seem to be obtained by using only cells where IIF does not occur, i.e., the smaller cells of the size distribution reported in Figure 4a. Indeed, the experimental data shown in Figure 9 were originally obtained for analyzing the osmotic behavior (i.e., the determination of cell permeability) by following cell-size variations under a cryomicroscope. Thus, this common, experimental practice[29] determines the exclusion of the portion of data until IIF occurs.

It is now possible to explain the reason why our model, when the initial cell distribution of Figure 4a is accounted for, shows a reasonable predictive capabilities in a wide range of operative conditions, except for those ones adopted in Figure 9c–f. It should be noted in passing that, the fractional cell volume represents the entire cell-size distribution, i.e., it takes into account both small and large cells. Thus, when the interplay of water osmosis and IIF phenomena gives rise to different fates depending on cell size, the comparison between model results and experimental data limited to small size cells may not be successful. This is the case of Figure 9c–9f. Indeed, in these cases, according to the corresponding model results, the behavior of the small and large cells is quite different (cf. Figure 10a), and IIF involves a relevant portion of the size distribution of the cell population (cf. Figure 10b). Accordingly, in these cases, the calculated profile of the average fractional cell volume is affected by both the frozen and unfrozen portions of the cell-size distribution.

Concluding Remarks

In this work, a mathematical model able to take into account the effect of the size distribution naturally present in a cell population suspension subjected to a standard cryoconservation protocol is proposed. In particular, a PB approach for the cell-size distribution is coupled to Mazur's water osmosis equation, and a discrete modeling approach for nucleation and diffusion-limited growth of ice crystals. The adjustable model parameters are determined by fitting the cryomicroscopically measured cumulative probability of internal ice formation as a function of temperature. Then, model reliability has been tested by predicting system behavior at different operative conditions.

It is found that, differently sized cells in a population exhibit a different IIF temperature under the same operative conditions. Specifically, the temperature of IIF is higher for larger cells. On the basis of this result, it is concluded that, if, in the absence of CPA, a relatively high-linear cooling rate is applied in a cryoconservation protocol, small and large cells in a population of the same lineage may behave quite differently, being the larger ones more prone to form internal, lethal ice. Thus, cell-size distribution needs to be taken into account when developing standard cryopreservation protocols. Indeed, post thaw viability of a cell population characterized by a relatively wide-size distribution may refer only to the small cells initially present, due to the selective IIF that preferentially kills large cells.

Along these lines of inquiry, the effect of CPAs on cryopreservation protocols of differently sized cells population will be analyzed in a subsequent work, where the implications and usefulness of the model will be clarified in terms of practical cryopreservation procedures.

Acknowledgments

S. Fadda would like to acknowledge the PhD School of Industrial Chemistry and Chemical Engineering of Politecnico di Milano, Italy. The financial support of BT (Biomedical Tissues) Srl, Sestu (CA), Italy is gratefully acknowledged.

Notation

a_0 = apparent hydrodynamic radius of water molecules in Eq.19, m
A_w = parameter in Eq. 22, $kg \cdot m^{-1} \cdot s^{-1}$
$A(t)$ = Cell membrane surface area, m^2
B = constant cooling rate, $K \cdot s^{-1}$
$B_0(t)$ = ice nucleation rate, s^{-1}
c_0 = isotonic salt concentration of cytoplasm, mol $\cdot m^{-3}$
$D(t)$ = water-diffusion coefficient in the cytoplasm, $m^2 \cdot s^{-1}$
$\overline{D}(t)$ = average water-diffusion coefficient, $m^2 \cdot s^{-1}$
$D_{eq}(t)$ = water-diffusion coefficient in the cytoplasm at equilibrium, $m^2 \cdot s^{-1}$
E = apparent activation energy for membrane permeation, $J \cdot \text{mol}^{-1}$
E_N = activation energy of nucleation, J
$G_v(t)$ = cell growth rate, $m^3 \cdot s^{-1}$
h = effective number of water molecules in the salt molecule hydration shell
$J(t)$ = ice nucleation rate per unit liquid solution volume, $m^3 \cdot s^{-1}$
J_0 = pre-exponential factor of nucleation rate, m^{-4}
k_B = Boltzmann's constant, $J\ K^{-1}$
k_e = Einstein's shape factor
L = cell diameter, m
$L_p(t)$ = effective membrane permeability, $m^3 \cdot N^{-1} \cdot s^{-1}$
$L_{p,ref}$ = effective membrane permeability at reference temperature T_{ref}, $m^3 \cdot N^{-1} \cdot s^{-1}$
MW_{H_2O} = molecular weight of water, $g \cdot \text{mol}^{-1}$
MW_{NaCl} = molecular weight of NaCl salt, $g \cdot \text{mol}^{-1}$
$n(V;t)$ = cell-number density distribution, m^{-3}
$n^0(V)$ = initial cell-number density distribution, m^{-3}
$n_1^0(V)$ = narrow-number density distributions of fictitious population of small cells, m^{-3}
$n_2^0(V)$ = narrow-number density distributions of fictitious population of large cells, m^{-3}
n_{NaCl} = number of salt moles inside a cell
$N_{ice}(t)$ = truncated, integer number of ice crystals in a cell
$\overline{N}_{ice}(t)$ = number of ice crystals in a cell
$N^0(L)$ = initial cell number histogram distribution
N_{tot}^0 = total number of cells
$PIIF(T)$ = probability of intracellular ice formation
Q = hydrodynamic interaction constant
$r_i(t)$ = radius of the i-th intracellular ice crystal, m
$r^*(t)$ = critical radius of ice nucleation, m
$\Re$ = universal gas constant, $J \cdot \text{mol}^{-1} \cdot K^{-1}$
$S_{NaCl}^{int}(t)$ = liquid intracellular salt wt %
$S_{eq}(t)$ = Liquid salt wt % at equilibrium
t = time, s
$T(t)$ = temperature, K

T_e = eutectic temperature of the binary water-NaCl system, K
T_{seed} = seeding temperature of extracellular ice, K
v_b = osmotically inactive cell volume fraction
V_{ice} = ice molar volume, $m^3 \cdot \text{mol}^{-1}$
v_{H_2O} = water molar volume, $m^3 \cdot \text{mol}^{-1}$
v_{NaCl} = salt molar volume, $m^3 \cdot \text{mol}^{-1}$
$V(t)$ = total cell volume, m^3
V_b = osmotically inactive cell volume, m^3
$V_{\text{ice}}(t)$ = intracellular ice volume, m^3
V_{NaCl} = intracellular salt volume, m^3
$V_{\text{water}}(t)$ = intracellular liquid water volume, m^3
V_0 = initial, isotonic cell volume, m^3
$x^{\text{int}}_{H_2O}(t)$ = intracellular liquid water molar fraction
$x^{eq}_{H_2O}(t)$ = liquid water molar fraction at the equilibrium
$x^{ext}_{H_2O}(t)$ = extracellular liquid water molar fraction

Greek letters

γ = surface energy for ice nucleation rate, $J \cdot m^{-2}$
φ = dissociation constant for salt in water
$\phi_s(S^{\text{int}}_{NaCl})$ = volume fraction of hydrated salt ions in cytoplasmatic solution
$\eta(t)$ = cytoplasmatic solution viscosity, $kg \cdot m^{-1} \cdot s^{-1}$
$\eta_{\text{ice}}(t)$ = intracellular ice volume percentage
$\eta_w\ (T)$ = pure water viscosity, $kg \cdot m^{-1} \cdot s^{-1}$
μ = parameter in Eq. 22
ρ_{H_2O} = pure water mass density, $g \cdot m^{-3}$
$\Omega_g(t)$ = ice growth driving force

Literature Cited

1. Mazur P. Kinetics of water loss from cells at subzero temperatures and likelihood of intracellular freezing. *J Gen Physiol*. 1963;47:347–369.
2. Karlsson JOM, Toner M. *Cryopreservation*. In: Lanza R, Langer R, Vacanti J, eds. *Principles of Tissue Engineering*. 2nd ed. San Diego: Academic Press, Inc; 2000:293–306.
3. Mazur P, Leibo SP, Chu EHY. A two-factor hypothesis of freezing injury. Evidence from Chinese Hamster tissue-culture cells. *Exp Cell Res*. 1972;71:345–355.
4. Karlsson JOM., Cravalho EG, Toner M. Intracellular ice formation: causes and consequences. *Cryoletters*. 1993;14:323–336.
5. Mazur P. Freezing of living cells: mechanisms and implications. *Am J Physiol*. 1984;247:C125–142.
6. Polge C, Smith AU, Parkes AS. Revival of spermatozoa after vitrification and dehydration at low temperatures. *Nature*. 1949;164:666.
7. Toner M, Cravalho EG, Karel M. Thermodynamics and kinetics of intracellular ice formation during freezing of biological cells. *J Appl Phys*. 1990;67:1582–1593.
8. Karlsson JOM, Cravalho EG, Toner M. A model diffusion-limited ice growth inside biological cells during freezing. *J Appl Phys*. 1994;75:4442–4445.
9. Zhao G, Luo D, Gao D. Universal model for intracellular ice formation and its growth. *AIChE J*. 2006;52:2596–2606.
10. Toner M, Tompkins RG, Cravalho EG, Yarmush ML. Transport phenomena during freezing of isolated hepatocytes. *AIChE J*. 1992;38:1512–1522.
11. Walcerz DB. Cryosim: A user-fryendly program for simulating cryopreservation protocols. *Cryobiol*. 1995;32:35–51.
12. Ramkrishna D. *Population Balances-Theory and Applications to Particulate Systems in Engineering*. San Diego: Academic Press, Inc; 2000.
13. Pegg DE. Simple equations for obtaining melting points and eutectic temperatures for the ternary system glycerol/sodium chloride/water. *Cryo Lett*. 1983;4:259–268.
14. Pegg DE. Equations for obtaining melting points and eutectic temperatures for the ternary system dimethyl sulfoxide/sodium chloride/water. *Cryo Lett*. 1986;7:387–394.
15. Levin RL, Cravalho EG, Huggins CE. A membrane model describing the effect of temperature on the water conductivity of erythrocyte membranes at subzero temperatures. *Cryobiology*. 1976;13: 415–429.
16. Dirksen JA, Ring TA. Fundamentals of crystallization: Kinetic effects on particle size distributions and morphology. *Chem Eng Sci*. 1991;46:2389–2427.
17. Zhang Y, Stangle GC. A micromechanistic model of microstructure development during the combustion synthesis process. *J Mater Res*. 1995;10:962–980.
18. Locci AM, Cincotti A, Delogu F, Orrù R, Cao G. Combustion synthesis of metal carbides: Part I. Model development. *J Mater Res*. 2005;20:1257–1268.
19. Vand V. Viscosity of solutions and suspensions. I. Theory. *J Phys Chem*. 1947a:277–299.
20. Vand V. Viscosity of solutions and suspensions. II. Experimental determination of the viscosity-concentration function of spherical suspensions. *J Phys Chem*. 1947b:300–314.
21. Vand V. Viscosity of solutions and suspensions. III. Theoretical interpretation of viscosity of sucrose solutions. *J Phys Chem*. 1947c:314–321.
22. Taborek P, Kleiman RN, Bishop DJ. Power-law behavior in the viscosity of supercooled liquids. *Phys Rev*. 1986;B34:183.
23. Karlsson JOM. Effect of solution composition on the theoretical prediction of the ice nucleation kinetics and thermodynamics. *Cryobiology*. 2009, In press. Available online. doi:10.1016/j.cryobiol.2009.07.004.
24. Schiesser WE. *The numerical method of lines*. San Diego: Academic Press, Inc; 1991.
25. Carnevale KA. Finite-Difference Model of Cell Dehydration during Cryopreservation. School of Mechanical Engineering, Georgia Institute of Technology; 2004. Thesis.
26. Perry RH, Green D. *Perry's Chemical Engineers' Handbook*. 6th ed. New York: McGraw-Hill; 1984.
27. McGrath JJ. Quantitative measurement of cell membrane transport: technology and applications. *Cryobiology*. 1997;34:315–334.
28. Elmoazzen HY, Chan CCV, Acker JP, Elliott JAW, McGann LE. The effect of cell distribution on predicted osmotic responses of cells. *Cryo Lett*. 2005;26:147–158.
29. Toner M, Cravalho EG, Stachecki J, Fitzgerald T, Tompkins RG, Yarmush ML, Armant DR. Nonequilibrium freezing of one-cell mouse embryos. Membrane integrity and developmental potential. *Biophys J*. 1993;64:1908–1921.

Manuscript received Jan. 30, 2009, and revision received Sept. 16, 2009.